JACS
JOURNAL OF THE AMERICAN CHEMICAL SOCIETY

Subscriber access provided by American Chemical Society

Article

# MOCVD-Derived Highly Transparent, Conductive Zinc- and Tin-Doped Indium Oxide Thin Films: Precursor Synthesis, Metastable Phase Film Growth and Characterization, and Application as Anodes in Polymer Light-Emitting Diodes

Jun Ni, He Yan, Anchuang Wang, Yu Yang, Charlotte L. Stern, Andrew W. Metz, Shu Jin, Lian Wang, Tobin J. Marks, John R. Ireland, and Carl R. Kannewurf

*J. Am. Chem. Soc.*, **2005**, 127 (15), 5613-5624• DOI: 10.1021/ja044643g • Publication Date (Web): 23 March 2005

**Downloaded from http://pubs.acs.org on March 25, 2009**

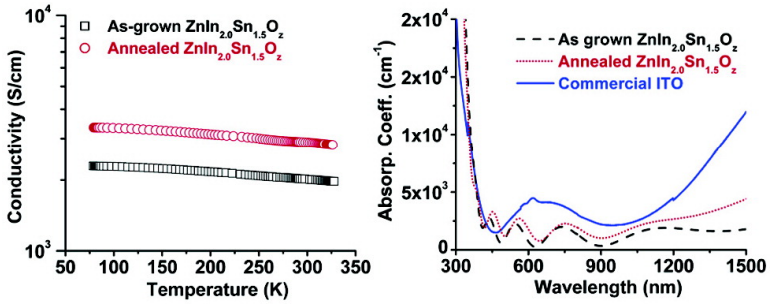


## More About This Article

Additional resources and features associated with this article are available within the HTML version:

- Supporting Information
- Links to the 4 articles that cite this article, as of the time of this article download
- Access to high resolution figures
- Links to articles and content related to this article
- Copyright permission to reproduce figures and/or text from this article

View the Full Text HTML

ACS Publications
High quality. High impact.

Journal of the American Chemical Society is published by the American Chemical Society. 1155 Sixteenth Street N.W., Washington, DC 20036

J|A|C|S
ARTICLES
Published on Web 03/23/2005

# MOCVD-Derived Highly Transparent, Conductive Zinc- and Tin-Doped Indium Oxide Thin Films: Precursor Synthesis, Metastable Phase Film Growth and Characterization, and Application as Anodes in Polymer Light-Emitting Diodes

Jun Ni,[†] He Yan,[†] Anchuang Wang,[†] Yu Yang,[†] Charlotte L. Stern,[†] Andrew W. Metz,[†] Shu Jin,[†] Lian Wang,[†] Tobin J. Marks,*[,†] John R. Ireland,[‡] and Carl R. Kannewurf[‡]

*Contribution from the Department of Chemistry, the Department of Electrical and Computer Engineering, and the Materials Research Center, Northwestern University, Evanston, Illinois 60208*

Received September 3, 2004; E-mail: t-marks@northwestern.edu

***Abstract:*** Four diamine adducts of bis(hexafluoroacetylacetonato)zinc [$Zn(hfa)_2$·(diamine)] can be synthesized in a single-step reaction. Single crystal X-ray diffraction studies reveal monomeric, six-coordinate structures. The thermal stabilities and vapor phase transport properties of these new complexes are considerably greater than those of conventional solid zinc metal−organic chemical vapor deposition (MOCVD) precursors. One of the complexes in the series, bis(1,1,1,5,5,5-hexafluoro-2,4-pentadionato)-(*N*,*N*′-diethylethylenediamine)zinc, is particularly effective in the growth of thin films of the transparent conducting oxide Zn−In−Sn−O (ZITO) because of its superior volatility and low melting point of 64 °C. ZITO thin films with In contents ranging from 40 to 70 cation % (a metastable phase) were grown by low-pressure MOCVD. These films exhibit conductivity as high as 2900 S/cm and optical transparency comparable to or greater than that of commercial Sn-doped indium oxide (ITO) films. ZITO films with the nominal composition of $ZnIn_{2.0}Sn_{1.5}O_z$ were used in fabrication of polymer light-emitting diodes. These devices exhibit light outputs and current efficiencies almost 70% greater than those of ITO-based control devices.

## Introduction

Transparent conducting oxide (TCO) thin films have wide applications in optoelectronics.[1,2] Although tin-doped indium oxide (ITO) is the current TCO of choice in most industrial applications, it has many limitations such as modest conductivity (2000−4000 S/cm for polycrystalline thin films), a relatively low work function (∼4.5 eV), and significant optical absorption in the blue-green spectral region. Note also that indium is in relative short supply and therefore expensive,[3] presenting significant challenges to large-scale introduction of next-generation flat panel display and photovoltaic technologies. Intense efforts are therefore being made to discover low In content alternative TCO materials with improved electrical and optical properties. New TCO materials such as Zn−In−O,[4−7] Al−Zn−O,[8] In−Cd−O[9−11] ternary systems, Zn−In−Sn−O (ZITO),[4,12−15] and Cd−In−Sn−O[10,16] quaternary systems are being actively investigated in thin film and/or bulk form.

[†] Department of Chemistry and the Materials Research Center.
[‡] Department of Electrical and Computer Engineering and the Materials Research Center.

(1) (a) Granqvist, C. G. *Adv. Mater.* **2003**, *15*, 1789. (b) Granqvist, C. G. *Appl. Phys. A* **1991**, *52*, 83. (c) Jarzebski, Z. M. *Phys. Status Solidi A* **1982**, *71*, 13. (d) Ohta, H.; Hosono, H. *Mater. Today* **2004**, *7*, 42.
(2) Ginley, D. S.; Bright, C. *MRS Bull.* **2000**, *25*, 15.
(3) Jansseune, T. *Compound Semiconductor Magazine*, Sept 2003.
(4) Phillips, J. M.; Cava, R. J.; Thomas, G. A.; Carter, S. A.; Kwo, J.; Siegrist, T.; Krajewski, J. J.; Marshall, J. H.; Peck, W. F.; Rapkine, D. H. *Appl. Phys. Lett.* **1995**, *67*, 2246.
(5) Moriga, T.; Edwards, D. D.; Mason, T. O.; Palmer, G. B.; Poeppelmeier, K. R.; Schindler, J. L.; Kannewurf, C. R.; Nakabayashi, I. *J. Am. Ceram. Soc.* **1998**, *81*, 1310.
(6) Yan, Y.; Pennycook, S. J.; Dai, J.; Chang, R. P. H.; Wang, A.; Marks, T. J. *Appl. Phys. Lett.* **1998**, *73*, 2585.
(7) Wang, A. C.; Dai, J. Y.; Cheng, J. Z.; Chudzik, M. P.; Marks, T. J.; Chang, R. P. H.; Kannewurf, C. R. *Appl. Phys. Lett.* **1998**, *73*, 327.
(8) (a) Hiramatsu, M.; Imaeda, K.; Horio, N.; Nawata, M. *J. Vac. Sci. Technol., A* **1998**, *16*, 669. (b) Minami, T.; Nanto, H.; Takata, S. *Jpn. J. Appl. Phys., Part 2* **1984**, *23*, L280. (c) Wasa, K.; Hada, T.; Hayakawa, S. *Jpn. J. Appl. Phys.* **1971**, *10*, 1732.
(9) (a) Shannon, R. D.; Gillson, J. L.; Bouchard, R. J. *J. Phys. Chem. Solids* **1977**, *38*, 877. (b) Pisarkiewicz, T.; Zakrzewska, K.; Leja, E. *Thin Solid Films* **1987**, *153*, 479.
(10) Wu, X.; Coutts, T. J.; Mulligan, W. P. *J. Vac. Sci. Technol., A* **1997**, *15*, 1057.
(11) Wang, A.; Babcock, J. R.; Edleman, N. L.; Metz, A. W.; Lane, M. A.; Asahi, R.; Dravid, V. P.; Kannewurf, C. R.; Freeman, A. J.; Marks, T. J. *Proc. Natl. Acad. Sci. U.S.A.* **2001**, *98*, 7113.
(12) (a) Ambrosini, A.; Palmer, G. B.; Maignan, A.; Poeppelmeier, K. R.; Lane, M. A.; Brazis, P.; Kannewurf, C. R.; Hogan, T.; Mason, T. O. *Chem. Mater.* **2002**, *14*, 52. (b) Palmer, G. B.; Poeppelmeier, K. R.; Mason, T. O. *J. Solid State Chem.* **1997**, *134*, 192.
(13) Palmer, G. B.; Poeppelmeier, K. R.; Mason, T. O. *Chem. Mater.* **1997**, *9*, 3121.
(14) (a) Minami, T.; Kakumu, T.; Shimokawa, K.; Takata, S. *Thin Solid Films* **1998**, *317*, 318. (b) Wang, A.; Edleman, N. L.; Babcock, J. R.; Marks, T. J.; Lane, M. A.; Brazis, P. W.; Kannewurf, C. R. *Mater. Res. Soc. Symp. Proc.* **2000**, *607*, 345.
(15) Ambrosini, A.; Malo, S.; Poeppelmeier, K. R.; Lane, M. A.; Kannewurf, C. R.; Mason, T. O. *Chem. Mater.* **2002**, *14*, 58.
(16) Ko, D.; Poeppelmeier, K. R.; Kammler, D. R.; Gonzalez, G. B.; Mason, T. O.; Williamson, D. L.; Young, D. L.; Coutts, T. J. *J. Solid State Chem.* **2002**, *163*, 259.

Importantly, new TCO materials with improved optoelectronic properties could significantly impact the development of future solar cell and flat panel display technologies.

A number of known and new TCO materials are based on $In_2O_3$. $In_2O_3$ is a semiconductor with a band gap of ~3.75 eV[17] and has a cubic bixbyite crystal structure where every fourth anion site is vacant.[18] As prepared, $In_2O_3$ is usually nonstoichiometric ($In_2O_{3-\delta}$, $\delta \approx 0.01$) because of oxygen vacancies[19] that can act as doubly ionized donors and can contribute up to two electrons per vacancy to the conduction band. Thus, $In_2O_3$ thin films exhibit electrical conductivity varying from 300 S/cm to 4000 S/cm, depending on the deposition technique and substrate.[20] Various elements, such as Zn[4,5,7], Cd,[10] Sn,[21,22] and Ga,[23] have been incorporated into $In_2O_3$ to tailor the electrical and optical properties. The combinations of these dopants with $In_2O_3$ provide a broad array of new TCO materials to be studied and understood. Among them, the ZITO system is particularly interesting. The solubility limit for $SnO_2$ in $In_2O_3$ has been established to be ca. 6 cation % for the bulk material,[24] and the solubility of ZnO in $In_2O_3$ is even lower.[13] However, when ZnO and $SnO_2$ are cosubstitued into $In_2O_3$, their solubilities are increased dramatically, and the In content can be as low as 60 cation % in the cosubstituted bulk material without a second phase precipitating.[13,15] The conductivity and transparency of $ZnO/SnO_2$ cosubstituted bulk $In_2O_3$ are comparable to those of bulk ITO, while the band gap can be tuned by controlling the ZnO and $SnO_2$ content. Although the ZITO system has been extensively studied in the bulk form,[12,13,15] there have been relatively few studies of ZITO thin films.[4,14]

Metal−organic chemical vapor deposition (MOCVD) is an attractive growth process for oxide thin films because it offers good compositional control, simple equipment, and conformal coverage, and it can be readily scaled up for large-area depositions. It is also interesting to note that it is possible to grow metastable phases that do not exist in standard phase diagrams via MOCVD techniques.[11] For a successful MOCVD process, a volatile metal−organic precursor is necessary. Preferably the precursor should be a low-melting solid. While a solid precursor is easy to handle, transforming it to the liquid form in the operating film growth reactor reservoir affords a constant precursor surface area and far more stable vapor pressure. Although zinc is an important component in new TCO materials, current zinc precursors for MOCVD processes still suffer from either poor reproducibility in growth processes or chemical instability. Several zinc compounds, such as liquid diethyl zinc[25] and dimethyl zinc,[26] zinc acetate,[27] and $Zn(hfa)_2 \cdot 2H_2O$·polyether adducts (hfa = 1,1,1,5,5,5-hexafluoro-2,4-pentanedionato),[28] have been demonstrated as MOCVD precursors in the growth of zinc-containing oxide thin films. However, diethyl zinc and dimethyl zinc are volatile, pyrophoric liquids that must be handled in an inert atmosphere.[25,26] They are highly reactive materials and difficult to control in the deposition of multicomponent films. In the case of zinc acetate and $Zn(hfa)_2 \cdot 2H_2O$·polyether, the water of hydration must be removed before these precursors can be used effectively. The volatility of zinc acetate also decreases markedly over prolonged deposition runs.[27] $Zn(dpm)_2$ (dpm = 2,2,6,6-tetramethyl-3,5-pentanedionato) is another widely used MOCVD precursor that does not require a co-reactant or pretreatment.[7] However, it is a solid over a broad temperature range and suffers from sintering at elevated temperatures and during film growth runs. Sintering decreases the surface area of the solid precursor and thereby causes the flux of gaseous zinc species being transported to vary during the film growth process, seriously compromising film compositional control. In an effort to enhance precursor volatility and thermal stability by saturating the coordination sphere, our group developed a series of solid $Zn(dpm)_2$·diamine adducts to address the deficiencies of current-generation Zn precursors.[29] Since these compounds remain solids under typical MOCVD growth conditions, and since it is well-known that fluorinated substituent introduction effectively increases precursor volatility while reducing the melting points of typical neutrally charged coordination complexes and increasing the stability of ancillary ligand binding via enhanced Lewis acidity,[30] a new $Zn(hfa)_2$·diamine motif that is liquid under typical MOCVD conditions was targeted as an attractive candidate for Zn MOCVD.

In this contribution, we report the facile synthetic access to a new series of thermally stable bis(1,1,1,5,5,5-hexafluoro-2,5-pentanedionato)zinc diamine adducts that have greatly improved volatility characteristics versus conventional $Zn(dpm)_2$ and its derivatives, and then we demonstrate the use of lowest melting member of the series as a liquid precursor in the efficient MOCVD growth of Zn−In−Sn−O transparent conducting oxide thin films. We also discuss in detail the microstructural, electrical, and optical properties of the deposited films and how these properties correlate with film composition. It will be seen that this information provides useful insight into strategies for designing other $In_2O_3$-based TCO materials. Finally, the superior performance characteristics of polymer light-emitting diode (PLED) devices based on ZITO rather than on conventional ITO anodes are discussed.

## Experimental Section

**Reagents and Physical Measurements.** All reagents except those mentioned below were purchased from Aldrich. High purity zinc nitrate (99.998% metal basis) was purchased from Alfa Aesar. ITO thin films


(17) Weiher, R. L.; Ley, R. P. *J. Appl. Phys.* **1966**, *37*, 299.
(18) Marezio, M. *Acta Crystallogr.* **1966**, *20*, 723.
(19) (a) Bellingham, J. R.; Mackenzie, A. P.; Phillips, W. A. *Appl. Phys. Lett.* **1991**, *58*, 2506. (b) Fan, J. C. C.; Goodenough, J. B. *J. Appl. Phys.* **1977**, *48*, 3524. (c) Chase, A. B.; Tippins, H. H. *J. Appl. Phys.* **1967**, *38*, 2469. (d) Warschkow, O.; Ellis, D. E.; Gonzalez, G. B.; Mason, T. O. *J. Am. Ceram. Soc.* **2003**, *86*, 1700.
(20) (a) Prince, J. J.; Ramamurthy, S.; Subramanian, B.; Sanjeeviraja, C.; Jayachandran, M. *J. Cryst. Growth* **2002**, *240*, 142. (b) Taga, N.; Maekawa, M.; Shigesato, Y.; Yasui, I.; Kakei, M.; Haynes, T. E. *Jpn. J. Appl. Phys., Part 1* **1998**, *37*, 6524. (c) Tarsa, E. J.; English, J. H.; Speck, J. S. *Appl. Phys. Lett.* **1993**, *62*, 2332. (d) Pan, C. A.; Ma, T. P. *J. Electrochem. Soc.* **1981**, *128*, 1953.
(21) Hamberg, I.; Granqvist, C. G. *J. Appl. Phys.* **1986**, *60*, R123.
(22) Maruyama, T.; Fukui, K. *J. Appl. Phys.* **1991**, *70*, 3848.
(23) (a) Cava, R. J.; Phillips, J. M.; Kwo, J.; Thomas, G. A.; Vandover, R. B.; Carter, S. A.; Krajewski, J. J.; Peck, W. F.; Marshall, J. H.; Rapkine, D. H. *Appl. Phys. Lett.* **1994**, *64*, 2071. (b) Wang, A. C.; Edleman, N. L.; Babcock, J. R.; Marks, T. J.; Lane, M. A.; Brazis, P. R.; Kannewurf, C. R. *J. Mater. Res.* **2002**, *17*, 3155.
(24) (a) Enoki, H.; Echigoya, J.; Suto, H. *J. Mater. Sci.* **1991**, *26*, 4110. (b) Frank, G.; Kostlin, H.; Rabenau, A. *Phys. Status Solidi A* **1979**, *52*, 231.
(25) (a) Hu, J. H.; Gordon, R. G. *J. Appl. Phys.* **1992**, *71*, 880. (b) Smith, F. T. J. *Appl. Phys. Lett.* **1983**, *43*, 1108.
(26) Hu, J.; Gordon, R. G. *Mater. Res. Soc. Symp. Proc.* **1991**, *202*, 457.
(27) (a) Jain, S.; Kodas, T. T.; Hampden-Smith, M. *Chem. Vap. Deposition* **1998**, *4*, 51. (b) Mar, G. L.; Timbrell, P. Y.; Lamb, R. N. *Chem. Mater.* **1995**, *7*, 1890.
(28) Gulino, A.; Castelli, F.; Dapporto, P.; Rossi, P.; Fragala, I. *Chem. Mater.* **2000**, *12*, 548.
(29) Babcock, J. R.; Wang, A.; Edleman, N. L.; Benson, D. D.; Metz, A. M.; Metz, M. V.; Marks, T. J. *Mater. Res. Soc. Symp. Proc.* **2000**, *623*, 312.
(30) (a) Malandrino, G.; Castelli, F.; Fragala, I. L. *Inorg. Chim. Acta* **1994**, *224*, 203. (b) Purdy, A. P.; Berry, A. D.; Holm, R. T.; Fatemi, M.; Gaskill, D. K. *Inorg. Chem.* **1989**, *28*, 2799.

were purchased from Colorado Concept, LLC. Poly(3,4-ethylenedioxythiophene)polystyrenesulfonate (PEDOT-PSS) was purchased from H. C. Starck. All reagents were used as received. Elemental analyses were performed by Midwest Microlab, LLC. NMR spectra were recorded in $C_6D_6$ or $CDCl_3$ on a Varian Mercury 400 MHz spectrometer. Thermogravimetric analysis data were acquired on a TA instruments SDT 2960 DTA-TGA instrument under a nitrogen atmosphere at a pressure of 5.0 ± 0.1 Torr and with a temperature ramp rate of 1.5 °C/min.

Single crystal X-ray diffraction data and refinement details relating to the structure determinations for Zn complexes **1**, **3**, and **4** are summarized in Table S1 in Supporting Information. Data were collected on a CCD area detector diffractometer with graphite-monochromated Mo Kα radiation. Reflections were collected with a Bruker SMART detector and processed with SAINT-NT software from Bruker. Data were corrected for Lorentz and polarization effects. The structures were solved by direct methods and expanded using Fourier techniques. All non-hydrogen atoms were refined anisotropcally. Hydrogen atoms were introduced in idealized positions but were not refined. All calculations were performed using the Bruker SHELXTL crystallographic software package. All disordered atoms were refined with group anisotropic displacement parameters. The effect on the key metrical parameters of interest is negligible. The structure plots were produced using the ORTEP program.[31]

**Synthesis of Bis(1,1,1,5,5,5-hexafluoro-2,4-petanedionato)-(*N*,*N*,*N*′,*N*′-tetramethylethylenediamine)zinc, Zn(hfa)$_2$(TMEDA) (1).** To 1.00 g (3.36 mmol) of $Zn(NO_3)_2{\cdot}6H_2O$ dissolved in 60 mL of deionzed water was added 0.39 g (3.36 mmol) *N*,*N*,*N*′,*N*′-tetramethylethylenediamine. Next, 1.40 g (6.72 mmol) of 1,1,1,5,5,5-hexafluoro-2,4-pentanedione (Hhfa) was dissolved in 15 mL of absolute ethanol. To the ethanol solution, 0.40 g (6.72 mmol) of 1-propylamine was added dropwise over a period of 10 min. The ethanol solution was then slowly poured into the stirring Zn solution. The reaction mixture was stirred overnight, and the crude product was collected by filtration. The resulting white solid was dried over $P_2O_5$ and sublimed at 80 °C/$10^{-5}$ Torr. Yield: 1.26 g (63.2%). mp: 106−108 °C; Anal. Calcd. for $C_{16}H_{18}O_4N_2F_{12}Zn$: C, 32.26; H, 3.05; N, 4.70; Found: C, 32.11; H, 2.98; N, 4.60. $^1$H NMR ($C_6D_6$, $\delta$): 1.61 (s, 4H, $CH_2$), 1.79 (s, 12H, $CH_3$), 6.22 (s, 2H, COCHCO). $^{13}$C NMR ($C_6D_6$, $\delta$): 45.28 ($CH_3$), 46.17 ($NCH_2CH_2N$), 89.17 (CH), 118.68 (q, $J$ = 286.3, Hz, $CF_3$), 178.89 (q, $J$ = 33.6 Hz, CO).

**Synthesis of Bis(1,1,1,5,5,5-hexafluoro-2,4-pentanedionato)-(*N*,*N*,*N*′,*N*′-tetraethylethylenediamine)zinc, Zn(hfa)$_2$(TEEDA) (2).** This compound was synthesized and purified via an approach similar to that for **1**, starting with 1.00 g (3.36 mmol) of $Zn(NO_3)_2{\cdot}6H_2O$, 1.40 g (6.72 mmol) of Hhfa, 0.40 g (6.72 mmol) of 1-propylamine, and 0.58 g (3.36 mmol) of *N*,*N*,*N*′,*N*′-tetraethylethylenediamine. Yield: 1.36 g (62.2%). mp: 103−106 °C; Anal. Calcd. for $C_{20}H_{26}O_4N_2F_{12}Zn$: C, 36.85; H, 4.02; N, 4.30; Found: C, 36.77; H, 3.76; N, 4.33. $^1$H NMR ($C_6D_6$, $\delta$): 0.66 (t, 12H, $CH_3$), 1.92 (s, $NCH_2CH_2N$), 2.06 (m, 4H, $CH_3CH_aH_b$), 2.80 (m, 4H, $CH_3CH_aH_b$), 6.26 (s, 2H, COCHCO). $^{13}$C NMR ($C_6D_6$, $\delta$): 7.31 ($CH_3$), 38.34 ($CH_3CH_2$), 46.67 ($NCH_2CH_2N$), 88.46 (CH), 117.92 (q, $J$ = 286.1, Hz, $CF_3$), 179.15 (q, $J$ = 33.7 Hz, CO).

**Synthesis of Bis(1,1,1,5,5,5-hexafluoro-2,4-pentanedionato)(*N*,*N*′-diethylethylenediamine)zinc, Zn(hfa)$_2$(*N*,*N*′-DEA) (3).** This compound was synthesized and purified via an approach similar to that for **1**, starting with 1.00 g (3.36 mmol) of $Zn(NO_3)_2{\cdot}6H_2O$, 1.40 g (6.72 mmol) of Hhfa, 0.40 g (6.72 mmol) of 1-propylamine, and 0.39 g (3.36 mmol) of *N*,*N*′-diethylethylenediamine. Yield: 1.34 g (66.9%). mp: 64−66 °C; Anal. Calcd. for $C_{16}H_{18}O_4N_2F_{12}Zn$: C, 32.26; H, 3.05; N, 4.70; Found: C, 32.17; H, 2.96; N, 4.65. $^1$H NMR ($C_6D_6$, $\delta$): 0.56 (t, 6H, $CH_3$), 1.07 (br s, 2H, NH), 1.63 (br s, 2H, $CH_3CH_aH_b$), 1.93 (br s, 4H, $NCH_2CH_2N$), 2.48 (br s, 2H, $CH_3CH_aH_b$), 6.24 (s, 2H, COCHCO). $^{13}$C NMR ($C_6D_6$, $\delta$): 13.33 ($CH_3$), 44.20 ($CH_3CH_2$), 46.10 ($NCH_2CH_2N$), 89.57 (CH), 118.59 (q, $J$ = 285.7, Hz, $CF_3$), 179.30 (q, $J$ = 33.9 Hz, CO).

**Synthesis of Bis(1,1,1,5,5,5-hexafluoro-2,4-pentanedionato)(*N*,*N*-diethylethylenediamine)zinc, Zn(hfa)$_2$(*N*,*N*-DEA) (4).** This compound was synthesized and purified via an approach similar to that for **1**, starting with 1.00 g (3.36 mmol) of $Zn(NO_3)_2{\cdot}6H_2O$, 1.40 g (6.72 mmol) of Hhfa, 0.40 g (6.72 mmol) of 1-propylamine, and 0.39 g (3.36 mmol) of *N*,*N*-diethylethylenediamine. Yield: 1.13 g (56.4%). mp: 136−139 °C; Anal. Calcd. for $C_{16}H_{18}O_4N_2F_{12}Zn$: C, 32.26; H, 3.05; N, 4.70; Found: C, 32.03; H, 2.92; N, 4.58. NMR $^1$H ($C_6D_6$, $\delta$): 0.608 (t, 6H, $CH_3$), 0.88 (br s, 2H, $NH_2$), 1.67 (br s, 4H, $CH_2CH_3$), 2.044 (br s, 2H, $NCH_2CH_2NH_2$), 2.65 (br s, 2H, $NCH_2CH_2NH_2$), 6.25 (s, 2H, COCHCO). $^{13}$C NMR ($C_6D_6$, $\delta$): 7.07 ($CH_3$), 35.34 ($CH_3CH_2$), 44.90 ($CH_3CH_2NCH_2CH_2N$), 53.94 ($CH_2NH_2$), 88.59 (CH), 117.60 (q, $J$ = 286.6, Hz, $CF_3$), 178.21 (q, $J$ = 33.8 Hz, CO).

**Synthesis of Tris(2,2,6,6-tetramethyl-3,5-heptanedionato)indium, In(dpm)$_3$.** This compound was synthesized following a literature procedure.[32] mp: 169−172 °C. Anal. Calcd. for $C_{33}H_{57}O_6In$: C, 59.64; H, 8.64; Found: C, 59.25; H, 8.76. $^1$H NMR ($C_6D_6$, $\delta$): 1.19 (s, 54H, $CH_3$), 5.84 (s, 3H, COCHCO).

**Synthesis of Bis(2,4-pentanedionato)tin(II), Sn(acac)$_2$.** This compound was synthesized following a literature procedure.[33] bp: 94−96 °C/0.04 Torr. Anal. Calcd. for $C_{10}H_{14}O_4Sn$: C, 37.90; H, 4.45; Found: C, 38.37; H, 4.59. $^1$H NMR ($CDCl_3$, $\delta$): 1.65 (s, 12H, $CH_3$), 5.07 (s, 2H, COCHCO).

**Synthesis of Poly(9,9-dioctylfluorene), PFO.** This compound was synthesized following a literature procedure.[34,35] $M_n$: 54 700, $M_w$: 107 000, by GPC versus polystyrene standards. $^1$H NMR ($CDCl_3$, $\delta$): 0.81 (t, 6H), 1.13−1.25 (m, 24H), 2.10−2.17 (m, 4H), 7.84 (d, 2H), 7.68 (m, 4H).

**Film Growth and Characterization.** ZITO thin films were grown in the previously described cold wall MOCVD reactor.[36] The Corning 1737F glass substrates were sonicated first in hexane, then in acetone for 10 min before deposition. The precursor reservoirs containing Zn(hfa)$_2$(*N*,*N*′-DEA) (**3**), In(dpm)$_3$, and Sn(acac)$_2$ were maintained at what was found by experimentation to be optimal temperatures of 68 °C, 105 °C, and room temperature, respectively, with the high-purity Ar carrier gas flow rate over the range of 6−30 sccm. The composition of the ZITO films was controlled by varying the Ar carrier gas flow rates. The carrier gas was mixed with $O_2$ immediately upstream of the susceptor in the reactor, with an $O_2$ flow rate varying from 100 to 120 sccm. The optimal susceptor temperature was found, after some experimentation, to be 500 °C with an operating system pressure of ca. 3 Torr throughout film growth process. The film growth rate is estimated to be ca. 3 nm/min under these conditions. Annealing of the as-grown ZITO films was performed in the same reactor at 500 °C for 1.5 h under vacuum (pressure < 0.01 Torr). X-ray $\theta-2\theta$ scans (XRD) of the MOCVD-derived ZITO films were performed on a Rigaku DMAX-A powder diffractometer using Ni-filtered Cu Kα radiation calibrated with Si powder sprinkled on the film surface. Transmission electron microscopic (TEM) images were obtained on a Hitachi 8100 microscope operating at 200 keV. Optical transmission data were recorded on a Cary 500 UV−vis−NIR spectrometer from 300 to 3300 nm with an uncoated Corning 1737F glass substrate as reference. Film

(31) Burnett, M. N.; John, C. K. *ORTEP III*; Report ORNL-6895; Oak Ridge National Laboratory: Oak Ridge, TN, 1996.

(32) (a) Jablonski, Z.; Rychlowska-Himmel, I.; Dyrek, M. *Spectrochim. Acta, Part A* **1979**, *35*, 1297. (b) Utsunomi, K. *Bull. Chem. Soc. Jpn.* **1971**, *44*, 2688.

(33) (a) Ewings, P. F. R.; Harrison, P. G.; Fenton, D. E. *J. Chem. Soc., Dalton Trans.* **1975**, 821. (b) Bos, K. D.; Budding, H. A.; Bulten, E. J.; Noltes, J. G. *Inorg. Nucl. Chem. Lett.* **1973**, *9*, 961.

(34) Yan, H.; Huang, Q. L.; Cui, J.; Veinot, J. G. C.; Kern, M. M.; Marks, T. J. *Adv. Mater.* **2003**, *15*, 835.

(35) Lim, E.; Jung, B.; Shim, H. *Macromolecules* **2003**, *36*, 4288.

(36) Hinds, B. J.; McNeely, R. J.; Studebaker, D. B.; Marks, T. J.; Hogan, T. P.; Schindler, J. L.; Kannewurf, C. R.; Zhang, X. F.; Miller, D. J. *J. Mater. Res.* **1997**, *12*, 1214.

***Scheme 1.*** Synthesis of $Zn(hfa)_2$·Diamine Complexes

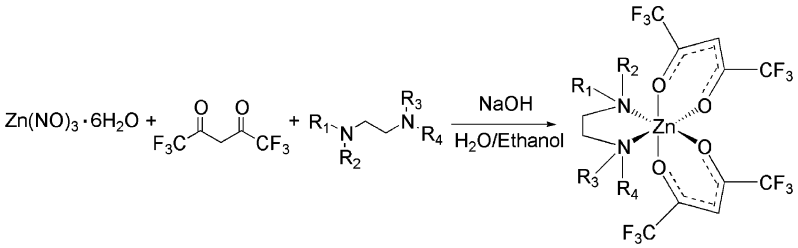


| Abbreviations | $R_1$ | $R_2$ | $R_3$ | $R_4$ | Melting Point (°C) |
|---|---|---|---|---|---|
| $Zn(hfa)_2$(TEMDA) **(1)** | $CH_3$ | $CH_3$ | $CH_3$ | $CH_3$ | 106-108 |
| $Zn(hfa)_2$(TEEDA) **(2)** | $CH_2CH_3$ | $CH_2CH_3$ | $CH_2CH_3$ | $CH_2CH_3$ | 103-106 |
| $Zn(hfa)_2$(*N*, *N*′-DEA) **(3)** | $CH_2CH_3$ | H | $CH_2CH_3$ | H | 64-66 |
| $Zn(hfa)_2$(*N*, *N*-DEA) **(4)** | $CH_2CH_3$ | $CH_2CH_3$ | H | H | 136-139 |

compositions were assayed using inductively coupled plasma atomic emission spectroscopy on an Atomscan 25 spectrometer after films were dissolved in hydrochloric acid. Film thickness was investigated with a Tencor P10 surface profiler after etching a step in the film with hydrochloric acid. The surface morphology of the ZITO films was investigated on a Digital Instruments Nanoscope III atomic force microsope (AFM) operating in the contact mode. Room-temperature four-probe charge transport data were acquired on a Bio-Rad HL5500 Hall effect measurement system at ambient temperature. Variable-temperature charge transport measurements were recorded between 77 and 330 K using instrumentation described previously.[37] X-ray photoelectron spectroscopy (XPS) of films was performed on an Omicron ESCAPROBE system using Al Kα radiation.

**Polymer Light-Emitting Diode Fabrication.** As-grown $ZnIn_{2.0}Sn_{1.5}O_z$ and commercial ITO substrates were first washed using a standard organic solvent and sonication procedure and then cleaned by a standard oxygen plasma treatment to remove surface contaminants.[38] This was immediately followed by spin-coating of a PEDOT-PSS solution. The resulting films (thickness: ∼50 nm) were dried in a vacuum oven at 150−200 °C for 1 h and then stored in an inert atmosphere glovebox before an ∼80-nm-thick PFO layer was spincast on them from a xylene solution. The resulting samples were then dried in a vacuum oven overnight. Inside an inert atmosphere glovebox, Ca was thermally evaporated on top of the PFO layer in a vacuum $<10^{-6}$ Torr, using a shadow mask to define the electrode area as 10 $mm^2$. Finally, an Al protective layer was thermally deposited on top of the Ca layer.[34] The PLEDs were characterized under inert atmosphere inside a sealed aluminum sample container within 0.5 h after fabrication using instrumentation described elsewhere.[34]

## Results

In this section, the synthesis of a new series of $Zn(hfa)_2$·diamine MOCVD precursors is presented, as well as a discussion of their molecular structural and volatility characteristics. Also presented in this section are the microstructural, charge transport, and optical properties of ZITO thin films grown using one of the Zn precursors and then the successful implementation of the MOCVD-derived ZITO films as anodes in polymer blue light-emitting diodes.

**MOCVD Precursor Synthesis and Characterization.** Four $Zn(hfa)_2$·diamine complexes, in which the diamine ancillary ligands were varied in symmetry and lipophilicity, were synthesized in a straightforward single-step reaction under ambient conditions from commercially available reagents (Scheme 1). The products are insoluble in the $H_2O$/ethanol reaction solution and can be readily isolated by filtration. The complexes were then readily purified by sublimation under reduced pressure to yield white crystalline solids. Qualitatively, these complexes are found to be far more volatile than current-generation Zn precursors and are air- and moisture-stable. Melting point data are summarized in Scheme 1, and NMR data are summarized in the Experimental Section. Substitution of alkyl groups on diamine skeleton clearly leads to substantial variations in the melting points of these complexes, one of the goals of this investigation.

Single crystals of compounds **1**, **3**, and **4** were obtained from hexane solution by slow cooling. Single crystal X-ray diffraction experiments reveal that they are all monomeric (Figure 1). Despite the fact that these complexes are synthesized via an aqueous route, coordinated water is not observed, and in all three complexes, the $Zn^{2+}$ ion is surrounded by $\beta$-diketonate and diamine ligands in a quasi-octahedral six-coordinate geometry. N−Zn−N bond angles range from 84.60(16)° to 85.74(11)°, while trans ligand atom−Zn−ligand atom bond angles range from 166.68(10)° to 177.21(11)°, indicating significant distortion from an idealized octahedron. These structures stand in contrast to those of $Zn(hfa)_2$·$2H_2O$·polyether adducts in which the polyether does not bond directly to the $Zn^{2+}$ ion but instead interacts with coordinated water through hydrogen bonds.[28] This difference can be attributed to the fact that a diamine is a stronger Lewis base and competes more favorably with water for the $Zn^{2+}$ ion than does the polyether.

The Zn−N bond lengths in complex **1** are 2.145(1) Å and 2.151(1) Å, while in **3** they are 2.125(3) Å. The shorter Zn−N bond lengths in complex **3** can be attributed to the difference in bulkiness between *N*,*N*,*N*′,*N*′-tetraethylenediamine (TMEDA) and *N*,*N*′-dithylenediamine (*N*,*N*′-DEA) ligands. TMEDA, with four methyl groups on the two N atoms, incurs greater steric repulsion than does *N*,*N*′-DEA, which has an ethyl group and a proton on each N atom. The increased steric hindrance results in slightly longer Zn−N bonds. This is more clearly demonstrated in the structure of complex **4**. Because of the unsymmetrical nature of the *N*,*N*-diethylenediamine ligand in complex **4**, the Zn−$N(CH_2CH_3)_2$ bond undergoes significant lengthening (average length 2.185(3) Å), while Zn−$NH_2$ shortens (average

(37) Lyding, J. W.; Marcy, H. O.; Marks, T. J.; Kannewurf, C. R. *IEEE Trans. Instrum. Meas.* **1988**, *37*, 76.
(38) Malinsky, J. E.; Jabbour, G. E.; Shaheen, S. E.; Anderson, J. D.; Richter, A. G.; Marks, T. J.; Armstrong, N. R.; Kippelen, B.; Dutta, P.; Peyghambarian, N. *Adv. Mater.* **1999**, *11*, 227.

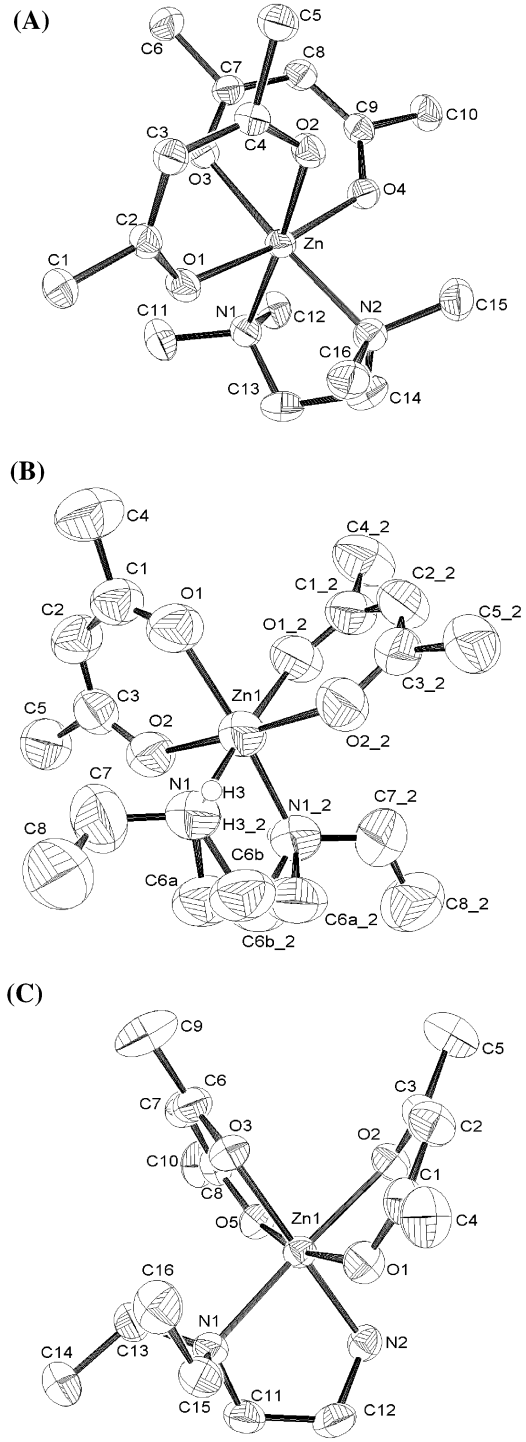


***Figure 1.*** ORTEP drawing (50% ellipsoid probability) of the molecular structures of complexes (A) $Zn(hfa)_2(TMEDA)$ (**1**), (B) $Zn(hfa)_2$(*N*,*N*′-DEA) (**3**), and (C) $Zn(hfa)_2$(*N*,*N*-DEA) (**4**). Hydrogen and fluorine atoms are omitted for clarity.

length 2.075(3) Å). Variations in Zn−N bond lengths also lead to variations in Zn−O bond lengths. In complex **4**, the Zn−O bond trans to the elongated Zn−N bond averages 2.181(2) Å, while the other five Zn−O bond lengths range from 2.083(2) to 2.117(2) Å. The Zn−O distances in complexes **1** and **3** also fall into this range, which is longer than the 2.06 Å reported for hydrated $Zn(hfa)_2$,[39] because of coordination of the ancillary diamine ligand. Selected bond lengths and angles are compiled in Table 1.

It is also interesting to compare the metrical parameters of complex **1**, $Zn(hfa)_2(TMEDA)$, to the structurally similar complex $Zn(dpm)_2(TMEDA)$,[29] where methyl groups replace the F atoms on the diketonate skeleton. In $Zn(dpm)_2(TMEDA)$, the average Zn−N bond length is 2.245(3) Å, significantly longer than the average Zn−N bond length found in **1**, 2.148(1) Å, while the average Zn−O bond length is 2.044(2) Å, much shorter than the average Zn−O bond length in **1** (2.109(1) Å). This variation in Zn-ligand contacts clearly demonstrates that the electron-withdrawing characteristics of the hfa ligand increase the Lewis acidity of $Zn^{2+}$ ion and in turn strengthen the bonding between the $Zn^{2+}$ center and the neutral ancillary ligands. The melting point of $Zn(dpm)_2(TMEDA)$ is reported to be 196−202 °C, about 90 °C higher than that of **1**, 106−108 °C. The significantly lower melting point of **1** can be attributed to, among other factors, the reduced intermolecular interactions in the fluorocarbon-substituted complex.[40]

Complex **4** has an abnormally high melting point and lower than average volatility (see below) than the other three complexes. Examination of a packing diagram (Figure 2) shows that these properties are likely due to extensive intermolecular hydrogen bonding. However, since protons bonded to the N atoms in complex **4** were not specifically located in the Fourier map, it is not possible to present a completely quantitative description of the hydrogen bonding metrical parameters. Nevertheless, careful examination of the packing diagram of complex **4** reveals close intermolecular proximity of N and O atom pairs on different molecules, with neighboring molecules paired together along the *c*-axis. The shortest intermolecular O···$H_2$N distance is 3.106 Å, and such short distances are indicative of relatively strong O···H···N hydrogen bonding.[41] Thus, at the molecular level, complex **4** is not a monomer, but crystallizes as a dimer bound via weak hydrogen bonds, which explains the high melting point and relatively low volatility of the solid. Although there exists an $-NH(CH_2CH_3)$ group in complex **3**, a similar proximity of N and O atoms is not observed and is explicable in terms of the steric encumbrance introduced by the ethyl group attached to each N atom in **3**. This steric screening doubtless prevents any close approach of neighboring molecules.

Reduced pressure thermogravimetric analysis (TGA) was performed on complexes **1**−**4** to investigate the volatility characteristics. Figure 3A compares weight loss properties of these complexes with the conventional Zn MOCVD precursor, $Zn(dpm)_2$. Although complex **2** appears to sublime with about 3% residue, which can be attributed to decomposition at elevated temperatures, all four complexes exhibit considerately greater volatility than $Zn(dpm)_2$. The smoothness of the curves also indicates that the coordinated diamine does not dissociate during heating. Figure 3B presents thermal activation plots of the sublimation rates. Clearly all four $Zn(hfa)_2$·diamine complexes have higher vaporization rates and lower vaporization activation energies than $Zn(dpm)_2$ under typical MOCVD reactor conditions.

(39) Adams, R. P.; Allen, H. C.; Rychlewska, U.; Hodgson, D. J. *Inorg. Chim. Acta* **1986**, *119*, 67.
(40) Belot, J. A.; Neumayer, D. A.; Reedy, C. J.; Studebaker, D. B.; Hinds, B. J.; Stern, C. L.; Marks, T. J. *Chem. Mater.* **1997**, *9*, 1638.
(41) Hamilton, W. C.; Ibers, J. A. *Hydrogen Bonding in Solids*; *Methods of Molecular Structure Determination (Frontiers in Chemistry)*; W. A. Benjamin: New York, 1968; p78.

***Table 1.*** Selected Bond Lengths (Å) and Bond Angles (deg) for Complexes **1**, **3**, and **4**

| 1 | | 3 | | 4 | |
|---|---|---|---|---|---|
| Zn−O(1) | 2.103(1) | Zn(1)−O(1) | 2.111(2) | Zn(1)−O(1) | 2.102(2) |
| Zn−O(2) | 2.112(1) | Zn(1)−O(2) | 2.095(2) | Zn(1)−O(2) | 2.166(2) |
| Zn−O(3) | 2.126(1) | Zn(1)−N(1) | 2.125(3) | Zn(1)−O(3) | 2.083(2) |
| Zn−O(4) | 2.096(1) | | | Zn(1)−O(5) | 2.113(2) |
| Zn−N(2) | 2.145(1) | | | Zn(1)−N(1) | 2.194(3) |
| Zn−N(1) | 2.151(1) | | | Zn(1)−N(2) | 2.074(3) |
| O(4)−Zn−O(1) | 173.65(4) | O(2)−Zn(1)−O(2)_2 | 176.89(11) | N(2)−Zn(1)−O(3) | 177.21(11) |
| O(4)−Zn−O(2) | 90.98(4) | O(2)−Zn(1)−O(1)_2 | 91.69(8) | N(2)−Zn(1)−O(1) | 92.71(11) |
| O(1)−Zn−O(2) | 85.06(4) | O(2)_2−Zn(1)−O(1)_2 | 86.02(8) | O(3)−Zn(1)−O(1) | 89.91(10) |
| O(4)−Zn−O(3) | 85.09(4) | O(2)−Zn(1)−O(1) | 86.02(8) | N(2)−Zn(1)−O(5) | 91.06(11) |
| O(1)−Zn−O(3) | 89.52(4) | O(2)_2−Zn(1)−O(1) | 91.69(8) | O(3)−Zn(1)−O(5) | 86.18(10) |
| O(2)−Zn−O(3) | 83.32(4) | O(1)_2−Zn(1)−O(1) | 85.15(12) | O(1)−Zn(1)−O(5) | 168.24(10) |
| O(4)−Zn−N(2) | 90.90(5) | O(2)−Zn(1)−N(1) | 94.52(10) | N(2)−Zn(1)−O(2) | 94.27(11) |
| O(1)−Zn−N(2) | 94.42(5) | O(2)_2−Zn(1)−N(1) | 87.79(10) | O(3)−Zn(1)−O(2) | 85.14(10) |
| O(2)−Zn−N(2) | 95.58(5) | O(1)_2−Zn(1)−N(1) | 173.79(10) | O(1)−Zn(1)−O(2) | 82.34(10) |
| O(3)−Zn−N(2) | 175.82(5) | O(1)−Zn(1)−N(1) | 95.46(11) | O(5)−Zn(1)−O(2) | 86.28(10) |
| O(4)−Zn−N(1) | 94.00(5) | O(2)−Zn(1)−N(1)_2 | 87.79(10) | O(3)−Zn(1)−N(1) | 95.92(10) |
| O(1)−Zn−N(1) | 89.85(5) | O(2)_2−Zn(1)−N(1)_2 | 94.52(10) | O(1)−Zn(1)−N(1) | 93.31(11) |
| O(2)−Zn−N(1) | 174.83(4) | O(1)_2−Zn(1)−N(1)_2 | 95.46(10) | O(5)−Zn(1)−N(1) | 98.12(11) |
| O(3)−Zn−N(1) | 95.71(5) | O(1)−Zn(1)−N(1)_2 | 173.79(10) | O(2)−Zn(1)−N(1) | 175.52(10) |
| N(2)−Zn−N(1) | 85.74(5) | N(1)−Zn(1)−N(1)_2 | 84.60(16) | N(2)−Zn(1)−N(1) | 84.88(11) |

**ZITO Film Growth and Characterization.** Complex **3** was chosen as the optimum Zn precursor for the subsequent MOCVD growth of Zn−In−Sn−O thin films because it has the lowest melting point. Under typical growth conditions, complex **3** should be a liquid in the thermostated MOCVD reactor precursor reservoir. Being a liquid under these conditions affords essentially constant surface area and vaporization rate, which are found to significantly improve compositional reproducibility in film growth.[40]

The two growth parameters that affect the film properties most, aside from precursor delivery rates, are growth temperature and $O_2$ flow rate. The present ZITO films were grown over a temperature range of 350−535 °C. It is found that when the growth temperature is below 420 °C, the films are largely amorphous and often opaque. Films deposited between 420 and 470 °C are crystalline; however, the carbon content is high (>5% by XPS) because of incomplete decomposition of the organic species. Films deposited above 510 °C have very low Sn contents because the $Sn(acac)_2$ precursor decomposes before reaching the reactor film growth area. In the present reactor, the optimal temperature window for ZITO film growth is found to be 470−510 °C. In general, higher temperatures afford lower carbon contamination and higher crystallinity of deposited ZITO films. At 500 °C, which is the upper limit of the deposition temperature window, good composition control is still achievable. Thus, 500 °C was selected as the optimum growth temperature for the ZITO films discussed in this contribution.

In ZITO film growth, when the $O_2$ partial pressure is low, the deposited films are not transparent and are morphologically rough because of incomplete precursor decomposition. When the $O_2$ partial pressure is high, the charge carrier concentration and conductivity of the deposited films are low, presumably because of filling of oxygen vacancies in the $In_2O_3$ matrix. The $O_2$ partial pressure was optimized by depositing films at various $O_2$ flow rates, and 2.0−2.4 Torr was found to yield the most crystalline, transparent, smooth, and conductive films.

Using $Zn(hfa)_2$(*N*,*N*′-DEA) (**3**), $In(dpm)_3$, and $Sn(acac)_2$ as precursors, we grew films with the nominal composition $ZnIn_xSn_yO_z$ ($1.5 < x < 4.0$, $0.5 < y < 2.5$) on Corning 1737F glass substrates at 500 °C. Since XPS qualitatively reveals that these

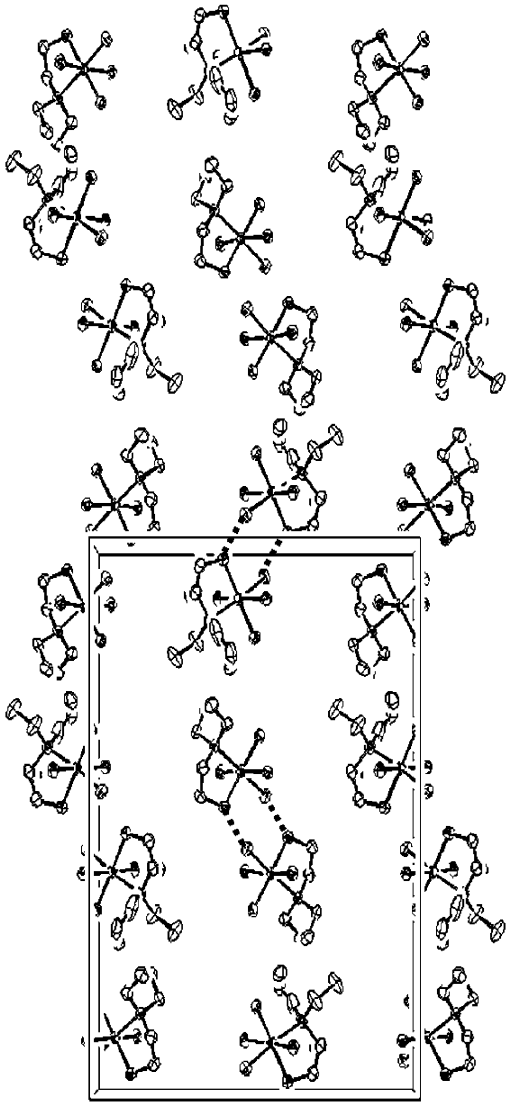

***Figure 2.*** Packing diagram of complex **4** viewed along the *c*-axis. Carbon atoms on diketonate ligands and fluorine and hydrogen atoms are omitted for clarity. Dotted lines connect the nearest hydrogen-bonded O and $NH_2$ groups. The distance is 3.106 Å.

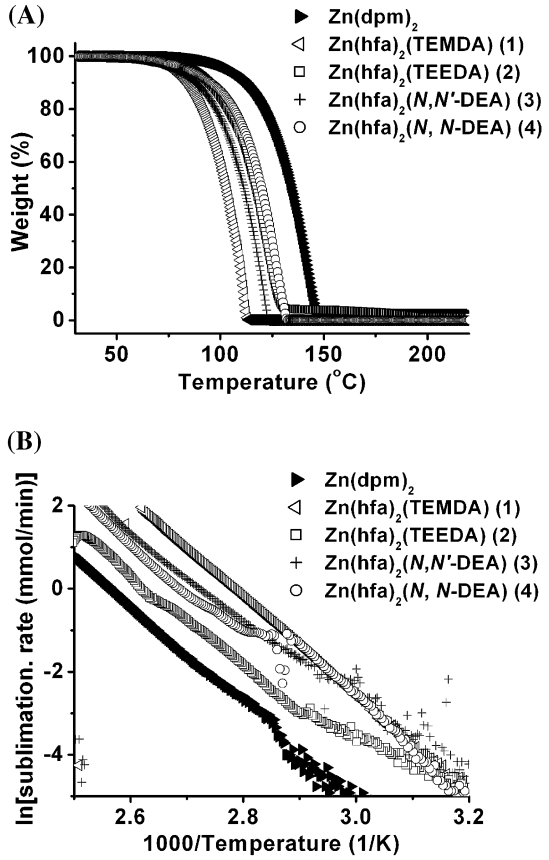


***Figure 3.*** (A) Low-pressure TGA comparison of the volatilities of the Zn(hfa)$_2$·diamine series and Zn(dpm)$_2$. (B) Thermal activation volatility comparison of the Zn(hfa)$_2$·diamine series and Zn(dpm)$_2$.

films are oxygen-deficient, as is the case in the ZITO bulk material,[15] and since the oxygen content varies from film to film, oxygen stoichiometry in the films discussed here is simply referred to as "*z*" in the formula, as is standard practice for other TCO materials.[2,15]

It is found by XRD (Figure 4) that at high In content, the MOCVD-derived ZITO films can be clearly indexed in the $In_2O_3$ bixbyite structure (JCPDS Card No. 06-416). The predominant (222) and (400) reflections indicate some degree of texturing of the films on the glass substrate. As the In content is decreased, the reflections broaden, and finally, when Zn and Sn reach the solubility limit at about $x = 1.8$ and $y = 1.7$, the characteristic reflections of the ZnO and/or $SnO_2$ phases appear in the XRD patterns. The lowest In content for which the films retain a phase-pure bixbyite structure is found to be a remarkable ca. 40 cation %, while in commercial ITO thin films the In content is near 90 cation %. The present results are in agreement with the bulk phase findings of Peoppelmeier et al. that cosubstitution of Zn with Sn in $In_2O_3$ dramatically increases the solubility of both $SnO_2$ and ZnO.[13] In the present contribution, we will only discuss phase-pure Zn- and Sn-doped $In_2O_3$ thin films, with an In content range of 40−70 cation %.

Four series of MOCVD-derived ZITO thin films are discussed below. Within each series, the Zn:In ratio is held constant while the Sn:Zn ratio is varied. The Zn:In ratio is then varied between series. These films all exhibit polycrystalline microstructures as evidenced by XRD and electron diffraction patterns. The plan-view TEM image of a structurally and electrically representative film reveals discrete grains with sizes ranging from 100 to 200

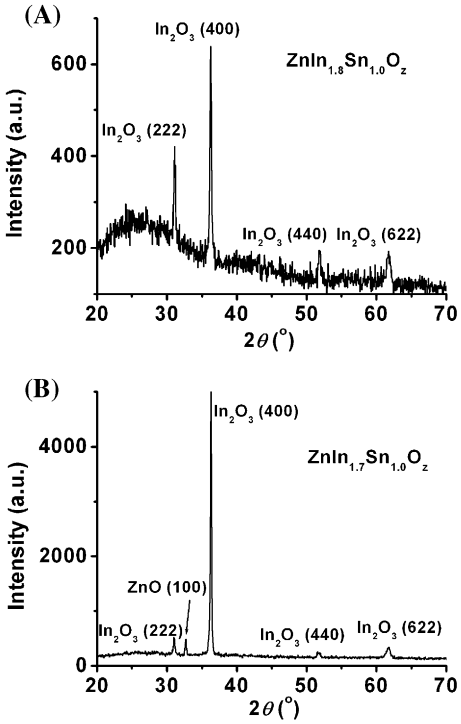


***Figure 4.*** (A) $\theta-2\theta$ X-ray diffraction scan of an MOCVD-derived $ZnIn_{1.8}Sn_{1.0}O_z$ film, showing the predominant $In_2O_3$ crystal structure. The broad peak between 22° and 28° is due to glass substrate. (B) $\theta-2\theta$ X-ray diffraction scan of a $ZnIn_{1.7}Sn_{1.0}O_z$ film, showing both doped $In_2O_3$ and ZnO phases.

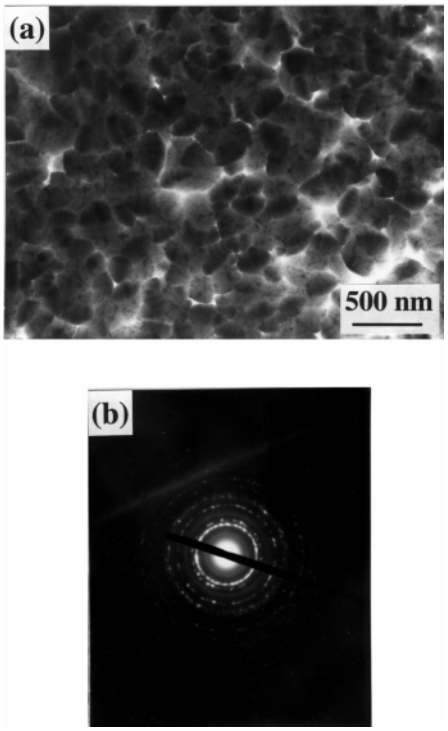


***Figure 5.*** (A) Plan-view TEM image of a $ZnIn_{2.0}Sn_{1.5}O_z$ film. (B) Corresponding electron diffraction pattern showing the $In_2O_3$ crystal structure.

nm (Figure 5), in good agreement with AFM and SEM data. The electron diffraction pattern is consistent with a randomly oriented $In_2O_3$ crystal structure. Deposited films are quite smooth by AFM, with root-mean-square (RMS) roughnesses no greater than 2% of the film thickness.

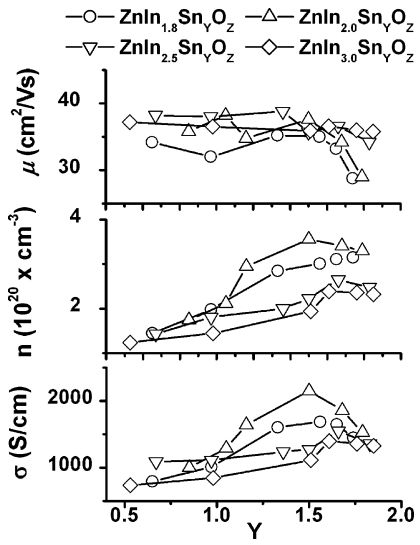


***Figure 6.*** Room temperature conductivity-composition, carrier concentration composition, and carrier mobility-composition plots of ZITO films. $\sigma$: conductivity; $n$: carrier concentration; $\mu$: carrier mobility. Lines through the data points are drawn as a guide to the eye.

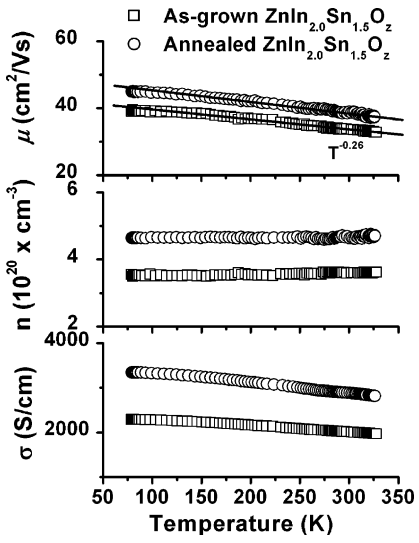


***Figure 7.*** Variable-temperature charge transport measurements on a typical MOCVD-derived ZITO ($ZnIn_{2.0}Sn_{1.5}O_z$) film before and after annealing in a vacuum at 500 °C for 1.5 h. $\sigma$: conductivity; $n$: carrier concentration; $\mu$: carrier mobility.

The electrical properties of the MOCVD-derived ZITO films are closely related to their chemical compositions (Figure 6; detailed room-temperature charge transport data are tabulated in Table S11 in Supporting Information). Conductivities first increase with addition of Sn, then decrease after reaching a maximum value. The film having the highest conductivity is found to have a nominal composition of $ZnIn_{2.0}Sn_{1.5}O_z$, with a conductivity of 2150 S/cm. All films are n-type, meaning that the majority carriers are electrons. Sn doping clearly leads to an increase in carrier concentration until the carrier concentration eventually reaches a maximum, and beyond that point, the carrier concentration either levels off or decreases slightly. While Sn doping generally increases the carrier concentration in these ZITO films, it has a negative overall impact on carrier mobility. In fact, both Zn and Sn doping lead to significant decrease in carrier mobility. Variable-temperature charge transport data for a representative ZITO film are shown in Figure 7. Both conductivity and carrier mobility decrease slightly as temperature increases from 78 to 330 K, revealing a modest "metal-like" charge transport behavior ($d\sigma/dT < 0$), while carrier concentration remains essentially constant. Carrier mobility is found to scale approximately as $T^{-0.26}$.

Regarding optical properties, the present MOCVD-derived ZITO films are highly transparent. All films exhibit 80% or greater transmittance between 400 and 1500 nm. The absorption coefficients of the ZITO films indicate that the transparency of these films is comparable to or greater than that of commercial ITO. The UV−vis−NIR spectrum of a representative ZITO film is presented in Figure 8. Note that ZITO is more transparent at shorter wavelengths and that the ZITO plasmon edge in the NIR, which is due to free carrier absorption and reflection, exhibits a significant red shift versus ITO. Band gaps of the films, estimated from plotting $(\alpha h\nu)^2$ against photon energy assuming a direct band gap,[42] vary from 3.65 to 3.90 eV (Table S11 in Supporting Information), falling within the 3.6−4.2 eV range reported for ITO. Note that the band gap generally increases with increasing carrier concentration, in accord with a Burstein−Moss shift (see below).

Annealing of the present ZITO films in a vacuum (pressure < 0.01 Torr) at 500 °C generally leads to a 20−40% increase in conductivity. Charge transport and optical data for a $ZnIn_{2.0}Sn_{1.5}O_z$ film before and after annealing are shown in Figures 7 and 8 and in Table 2. Annealing causes a slight increase in carrier mobility but a substantial jump in carrier concentration. As a result, the conductivity of $ZnIn_{2.0}Sn_{1.5}O_z$ increases from 2150 to 2890 S/cm. The annealed films also have a widened band gap and a blue shift of the plasmon edge compared to the as-grown films. The overall optical transmission of the annealed ZITO films decreases slightly (Figure 8).

**Chemical Reactivity of MOCVD-Derived ZITO Thin Films.** All of the MOCVD-derived ZITO films exhibit appreciable chemical inertness. It typically requires more than 1 h to dissolve a 200-nm-thick ZITO film in concentrated hydrochloric acid, while less than 15 min is required for a commercial 130-nm-thick ITO film. PEDOT-PSS is commonly used in PLED/organic light-emitting diodes (OLED) devices to improve hole injection and device performance.[43] It is well-established that since PEDOT-PSS is highly acidic (pH ≈ 1), it etches the anode (ITO) layer, a process that destabilizes the ITO/PEDOT-PSS interface and compromises charge injection.[44] Our experiments show that ZITO is significantly more resistant to PEDOT-PSS attack than ITO as assessed by the quantity of free In found in the PEDOT-PSS layer by XPS. A 50-nm layer of PEDOT-PSS was spin-cast on both a cleaned commercial ITO film and an MOCVD-derived $ZnIn_{2.0}Sn_{1.5}O_z$ film cleaned by same procedure. The two samples were subsequently placed into a vacuum oven at 200 °C for 1 h (common PEDOT-PSS curing conditions). Subsequent XPS measurements reveal that

(42) Metz, A. W.; Ireland, J. R.; Zheng, J. G.; Lobo, R. P. S. M.; Yang, Y.; Ni, J.; Stern, C. L.; Dravid, V. P.; Bontemps, N.; Kannewurf, C. R.; Poeppelmeier, K. R.; Marks, T. J. *J. Am. Chem. Soc.* **2004**, *126*, 8477.

(43) (a) Brown, T. M.; Kim, J. S.; Friend, R. H.; Cacialli, F. *Appl. Phys. Lett.* **1999**, *75*, 1679. (b) de Kok, M. M.; Buechel, M.; Vulto, S. I. E.; van de Weijer, P.; Meulenkamp, E. A.; de Winter, S. H. P. M.; Mank, A. J. G.; Vorstenbosch, H. J. M.; Weijtens, C. H. L.; van Elsbergen, V. *Phys. Status Solidi A* **2004**, *201*, 1342.

(44) (a) Wong, K. W.; Yip, H. L.; Luo, Y.; Wong, K. Y.; Lau, W. M.; Low, K. H.; Chow, H. F.; Gao, Z. Q.; Yeung, W. L.; Chang, C. C. *Appl. Phys. Lett.* **2002**, *80*, 2788. (b) de Jong, M. P.; van Ijzendoorn, L. J.; de Voigt, M. J. A. *Appl. Phys. Lett.* **2000**, *77*, 2255.

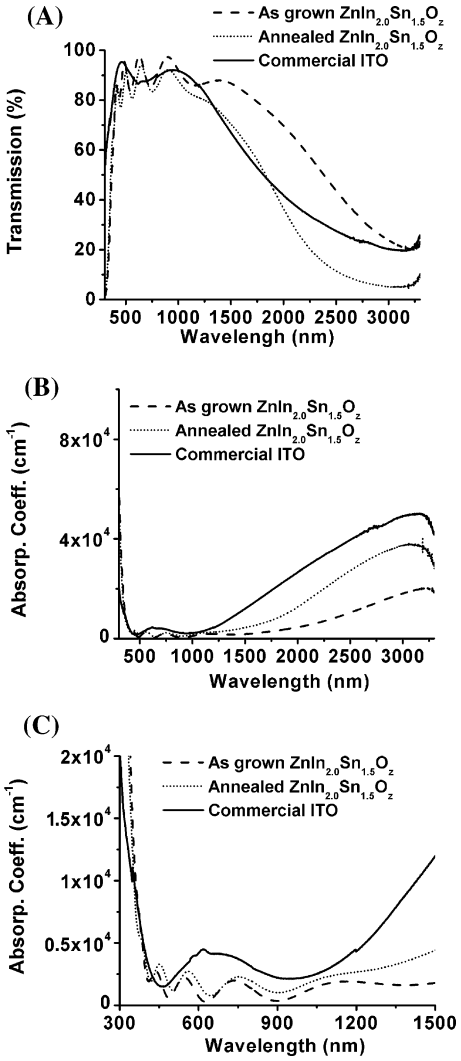


***Figure 8.*** (A) UV−vis−NIR spectra of an as-grown $ZnIn_{2.0}Sn_{1.5}O_z$ film, an annealed $ZnIn_{2.0}Sn_{1.5}O_z$ film, and a commercial ITO film. The ZITO film thickness is 340 nm; ITO film thickness is 130 nm. (B) Corresponding absorption coefficients as a function of wavelength plot. (C) Enlargement of (B) from 300 to 1500 nm.

***Table 2.*** Comparison of Room Temperature Charge Transport and Optical Properties of a $ZnIn_{2.0}Sn_{1.5}O_z$ Film before and after Annealing[a]

| $ZnIn_{2.0}Sn_{1.5}O_z$ | $\sigma_{298}$ (S/cm) | $\mu_{298}$ ($cm^2$/Vs) | $n_{298}$ ($10^{20}cm^{-3}$) | band gap (eV) |
|---|---|---|---|---|
| as-grown | 2150 | 37.4 | 3.56 | 3.88 |
| annealed | 2890 | 38.9 | 4.69 | 3.95 |

[a] $\sigma$: conductivity; $\mu$: carrier mobility; $n$: carrier concentration.

the In content at the surface of the PEDOT-PSS layer is ∼1.1 atomic % for the ITO-based sample and <0.05 atomic % for the $ZnIn_{2.0}Sn_{1.5}O_z$-based sample (Figure 9). Considering that the In content of $ZnIn_2Sn_{1.5}O_z$ is approximately half of that in ITO, the PEDOT-PSS dissolves >10× more ITO than it does $ZnIn_{2.0}Sn_{1.5}O_z$.

**Response Characteristics of ZITO-Based Polymer Blue Light-Emitting Diodes.** As-grown ZITO films with the nominal composition of $ZnIn_{2.0}Sn_{1.5}O_z$ were used as anodes in the fabrication of PLEDs because of their high conductivity. A control device with commercial ITO as the anode was also fabricated and evaluated at the same time under identical conditions. The structure of the PLED devices is shown in

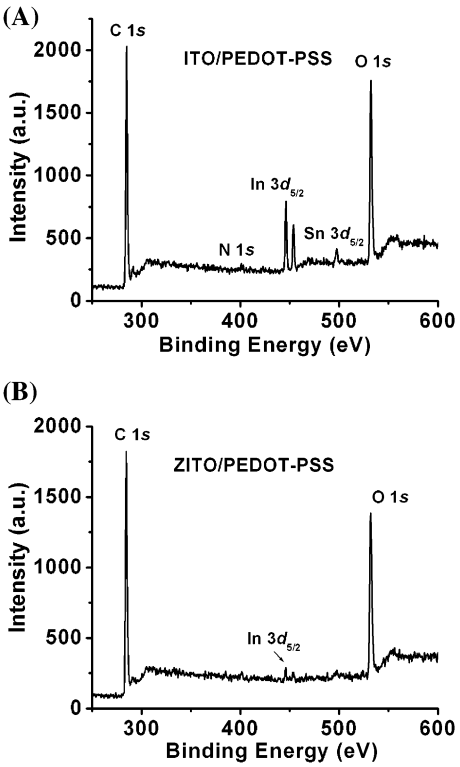


***Figure 9.*** Comparison of the XPS spectra of an ITO/PEDOT-PSS sample and a $ZnIn_2Sn_{1.5}O_z$/PEDOT-PSS sample. Note that after heating in a vacuum oven at 200 °C for 1 h, the $ZnIn_2Sn_{1.5}O_z$/PEDOT-PSS sample has significantly less In contamination than does the ITO/PEDOT-PSS sample. (A) ITO/PEDOT-PSS sample. (B) $ZnIn_2Sn_{1.5}O_z$/PEDOT-PSS sample.

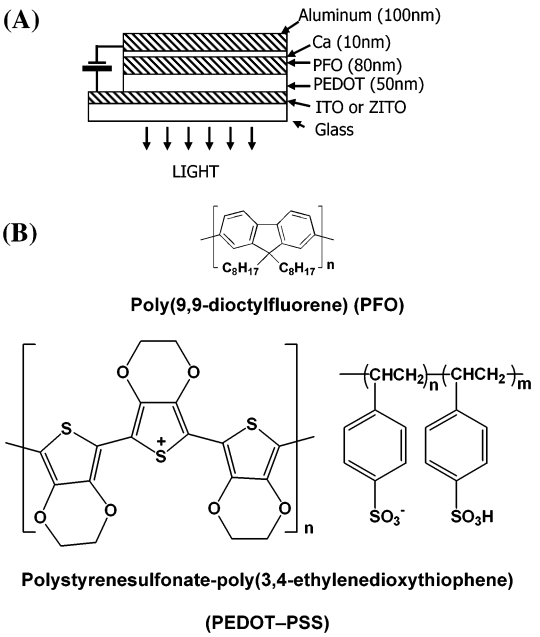


***Figure 10.*** (A) Structure of a PLED device. (B) Structures of PLED components PFO and PEDOT-PSS.

Figure 10. The emissive material in the devices is poly(9,9-dioctylfluorene), a blue light-emitting polymer. The response characteristics of this device and of the control device based on commercial ITO are presented in Figure 11. Both devices turn on at ∼4 V; however, the light output and current efficiency of the ZITO-based devices are as much as 70% greater than those of the ITO-based devices, while the current metrics of

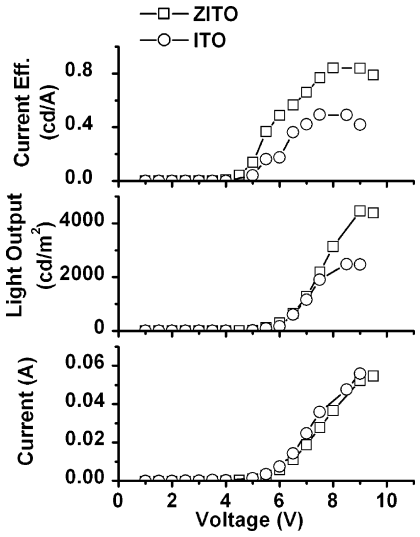


***Figure 11.*** Response of ITO-based vs ZITO-based PLED devices having the structure shown in Figure 10A. Lines through data points are drawn as a guide to the eye.

the two devices are comparable. At 9 V, the light output of the ZITO-based devices reaches a maximum of ~4500 cd/m$^2$, significantly greater than that of the ITO-based control devices and those of ITO-based blue light-emitting PLED devices reported in the literature employing PFO/PFO derivatives as the emissive layer.[45]

## Discussion

**Precursor Design and Synthesis.** Previously, $\beta$-diketonates, both fluorinated and fluorine-free, have been used extensively as supporting ligands in MOCVD precursors.[46] Because fluorinated substituents reduce cohesive intermolecular van der Waals interactions, complexes with fluorinated $\beta$-diketones are typically more volatile than the fluorine-free counterparts.[30,47] The electron-withdrawing characteristics of fluorocarbon substituents additionally increase the metal Lewis acidity and, hence, enhance the binding strengths of neutral ancillary ligands. The net consequence of combining fluorinated $\beta$-diketonates with neutral bases is to securely saturate the metal ion coordination sphere. This configuration effectively encapsulates the metal ion so that the possibility of volatility-degrading oligomerization or premature ligand dissociation is reduced. The result is monomeric structures with, in optimum cases, greatly improved thermal stability and volatility characteristics.[40,48] This effect is clearly reflected in the increased volatility and reduced melting points of complexes **1**, **2**, and **3** versus their nonfluorinated counterparts.[29] Combined with strong Lewis bases such as chelating amines, the fluorinated ligands enhance the thermal stability of the resulting complexes, which is particularly evident when comparing the thermal stability of the present Zn complexes with $Zn(hfa)_2 \cdot 2H_2O \cdot$polyether adducts.[28]

**ZITO Film Growth and Characterization.** One concern associated with the use of fluorinated MOCVD precursors is that the deposited films may contain $F^-$, either as a dopant or as a discrete fluoride-containing phase. Water is a commonly used co-reactant during MOCVD growth with fluorinated precursors to reduce unnecessary fluorine-containing products in MOCVD processes.[40,48,49] For the ZITO films discussed here, water was not used because the Sn precursor, $Sn(acac)_2$, is moisture-sensitive and undergoes rapid reaction with water before reaching the film growth area. Even without water, the deposited films exhibit no detectable fluoride phases in the XRD patterns. All films were also subjected to in-depth XPS analysis with sputter-cleaning of the surfaces. The fluoride content is found to be below the detection limits of the XPS instrumentation (<0.2 atomic %). Assuming in the extreme case of a 0.2 atomic % $F^-$ doping level with an unlikely 100% doping efficiency of carrier formation, the added carrier concentration resulting from $F^-$ doping alone is estimated to be $\sim 1.5 \times 10^{20}$ cm$^{-3}$. This quantity then represents the upper theoretical limit of ZITO free carrier concentration arising from $F^-$ doping in films with the maximum Zn content. Considering that in $F^-$ doped $In_2O_3$ films, the doping efficiency of fluorine is reported to vary from less than 1−10%,[50] the actual carrier concentration generated by $F^-$ in the present films should be at least 1 order of magnitude lower than the estimated maximum $F^-$ content. Therefore, compared to the ZITO carrier concentrations reported here, it is physically reasonable to assume that any additional carrier concentrations arising from adventitious $F^-$ and its variations due to the change in Zn precursor flow rate are insignificant. In the following discussion, trace fluoride influence on charge transport properties of the films is not considered. Note, however, that if there is in fact fluoride contamination, it should be beneficial to the properties of the films since it would be expected in most cases to increase the carrier concentration and thus the conductivity.

In bulk ZITO materials, a minimum In content of 60 cation % is required to retain the $In_2O_3$ bixbyite structure for Zn- and Sn-cosubstituted $In_2O_3$.[13] It is also possible to overdope a slight amount of Zn into the material without forming new phases.[15] The present study reveals that the solubility of ZnO and $SnO_2$ in $In_2O_3$ is much greater in MOCVD-derived films. Given the fact that the deposition conditions for these thin films (500 °C, 3 Torr working pressure) are far away from the thermodynamic equilibrium regime where ZITO bulk materials are typically synthesized (1100−1250 °C, 1 atm),[13] the MOCVD-derived

(45) (a) Shu, C.; Dodda, R.; Wu, F.; Liu, M.; Jen, A. *Macromolecules* **2003**, *36*, 6698. (b) Lee, J.; Cho, H.; Jung, B.; Cho, N.; Shim, H. *Macromolecules* **2004**, *37*, 8523. (c) Fung, M.; Lai, S.; Tong, S.; Chan, M.; Lee, S. T.; Wu, W. W.; Inbasekaran, M.; O'Brien, J. J. *Appl. Phys. Lett.* **2002**, *81*, 1497. (d) Brown, T. M.; Friend, R. H.; Millard, I. S.; Lacey, D. J.; Burroughes, J. H.; Cacialli, F. *Appl. Phys. Lett.* **2001**, *79*, 174. (e) Su, H.; Wu, F.; Shu, C. *Macromolecules* **2004**, *37*, 7197. (f) Pogantsch, A.; Wenzl, F. P.; List, E. J. W.; Leising, G.; Grimscale, A. C.; Mullen, K. *Adv. Mater.* **2002**, *14*, 1061. (g) Jiang, X.; Liu, S.; Ma, H.; Jen, A. *Appl. Phys. Lett.* **2000**, *76*, 1813.

(46) (a) Valet, M.; Hoffman, D. M. *Chem. Mater.* **2001**, *13*, 2135. (b) Malandrino, G.; Bettinelli, M.; Speghini, A.; Fragala, I. *Eur. J. Inorg. Chem.* **2001**, 1039. (c) Putkonen, M.; Sajavaara, T.; Johansson, L. S.; Niinisto, L. *Chem. Vap. Deposition* **2001**, *7*, 44. (d) Brooks, J.; Davies, H. O.; Leedham, T. J.; Jones, A. C.; Steiner, A. *Chem. Vap. Deposition* **2000**, *6*, 66. (e) Fleeting, K. A.; Davies, H. O.; Jones, A. C.; O'Brien, P.; Leedham, T. J.; Crosbie, M. J.; Wright, P. J.; Williams, D. J. *Chem. Vap. Deposition* **1999**, *5*, 261. (f) Krisyuk, V. V.; Turgambaeva, A. E.; Igumenov, I. K. *Chem. Vap. Deposition* **1998**, *4*, 43.

(47) (a) Sicre, J. E.; Dubois, J. T.; Eisentraut, K. J.; Sievers, R. E. *J. Am. Chem. Soc.* **1969**, *91*, 3476. (b) Springer, C. S.; Meek, D. W.; Sievers, R. E. *Inorg. Chem.* **1967**, *6*, 1105.

(48) (a) Babcock, J. R.; Wang, A. C.; Metz, A. W.; Edleman, N. L.; Metz, M. V.; Lane, M. A.; Kannewurf, C. R.; Marks, T. J. *Chem. Vap. Deposition* **2001**, *7*, 239. (b) Pollard, K. D.; Jenkins, H. A.; Puddephatt, R. J. *Chem. Mater.* **2000**, *12*, 701. (c) Gardiner, R.; Brown, D. W.; Kirlin, P. S.; Rheingold, A. L. *Chem. Mater.* **1991**, *3*, 1053.

(49) Pinkas, J.; Huffman, J. C.; Baxter, D. V.; Chisholm, M. H.; Caulton, K. G. *Chem. Mater.* **1995**, *7*, 1589.

(50) (a) Shigesato, Y.; Shin, N.; Kamei, M.; Song, P. K.; Yasui, I. *Jpn. J. Appl. Phys., Part 1* **2000**, *39*, 6422. (b) Mirzapour, S.; Rozati, S. M.; Takwale, M. G.; Marathe, B. R.; Bhide, V. G. *J. Mater. Sci.* **1994**, *29*, 700. (c) Maruyama, T.; Nakai, T. *J. Appl. Phys.* **1992**, *71*, 2915.

***Scheme 2.*** Dissociation of $(2Sn_{In}^{\bullet}O_i'')^x$ and Release of Free Carriers upon Annealing

$$(2Sn_{In}^{\bullet}O_i'')^x \longrightarrow 1/2O_2\,(g) + 2Sn^{\bullet} + 2e'$$

ZITO thin films are clearly composed of a metastable phase, a common observation in thin film synthesis by MOCVD.[11]

**ZITO Film Electrical and Optical Properties.** In ITO, carriers can be generated in two ways: (a) by oxygen vacancies and (b) by Sn doping.[51,52] In theory, each oxygen vacancy contributes two electrons while each $Sn^{4+}$ replacement for $In^{3+}$ contributes one electron. Note, however, that Sn doping efficiency is known to be low, and much of the Sn is postulated to form neutrally charged species that do not contribute free electrons.[51−53] Since in ZITO there is Zn as well as Sn doping, where each $Zn^{2+}$ theoretically contributes one hole, the carrier concentration in ZITO can be formally expressed as $[Sn_{In}^{\bullet}] - [Zn_{In}'] + 2n$, where $[Sn_{In}^{\bullet}]$ and $[Zn_{In}']$ are the concentrations of Sn and Zn that are electrically active, while $n$ is the concentration of oxygen vacancies. Note that, in the ZITO films investigated here, even at high Zn content ([Sn] < [Zn]) the majority carriers in all four ZITO series are still electrons. Any holes generated by Zn addition are apparently insufficient to offset electrons arising from Sn doping and oxygen vacancies. It has been proposed that not all Zn cations contribute holes, but rather some form neutral associates with oxygen vacancies such as $(2Zn_{In}'V_O^{\bullet\bullet})^x$, thus reducing the Zn doping efficiency.[15] The result is $[Zn_{In}'] < [Sn_{In}^{\bullet}] + 2n$, and the majority carriers are still electrons. This assertion is in good agreement with the findings in bulk ZITO materials and other *p*-doped $In_2O_3$ TCOs.[54] Thus, an increase in Sn content does not always lead to increases in carrier concentrations, as evident in Figure 6. At very high Sn contents, it is more likely for two Sn atoms to find neighboring sites and form neutral nonreducible $(Sn_2O_4)^x$ species. Under the film growth conditions discussed here, there should also be a significant quantity of Sn species forming another neutral oxide complex that fills empty anion sites in the $In_2O_3$ matrix: $(2Sn_{In}^{\bullet}O_i'')^x$.[51,53,54] The existence of $(2Sn_{In}^{\bullet}O_i'')^x$ is also supported by the annealing study, where heating ZITO films in a vacuum increases carrier concentration because of the release of $O_2$ from $(2Sn_{In}^{\bullet}O_i'')^x$ (Scheme 2). Therefore, beyond a critical point, introducing additional Sn does not increase the carrier concentration. Despite the high Sn doping level in the present ZITO system (Sn content ranging from 11 to 38 cation %) compared to that in typical ITO, the highest carrier concentration achieved in as-grown films is $3.56 \times 10^{20}$ $cm^{-3}$, substantially lower than the $8-10 \times 10^{20}$ $cm^{-3}$ value typically found in polycrystalline ITO films.[55] This is the result of both Zn doping and neutral species formation. While Zn doping neutralizes free electrons, formation of neutral species reduces the Sn doping efficiency.

In principle, carrier mobility is determined by a variety of carrier scattering mechanisms. Ionized impurity scattering (IIS) and lattice vibration scattering (LVS) are thought to be the more important scattering mechanisms in typical TCO materials. Grain boundary scattering (GBS) is only important in polycrystalline films having very small grain sizes.[42,53,56] The effect of neutral impurity scattering (NIS) on carrier mobility in TCOs is still a subject of debate.[53,54,56,57] The average grain size of the present ZITO films is estimated to be >100 nm from the electron microscopy and AFM images (see above), which is substantially larger than the estimated electron-mean-free path in typical TCO films, where it is ~10 nm.[56] For these reasons, we believe that in the MOCVD-derived ZITO films discussed here, GBS plays a minor role at most in carrier mobility. The fact that mobility scales only weakly with temperature ($\mu \propto T^{-0.26}$, Figure 7) shows that temperature-independent scattering mechanisms (IIS and/or NIS) play important roles in determining carrier mobility as do temperature-dependent LVS mechanisms. Our data show that doping of Zn and Sn generally has a negative effect on carrier mobility in ZITO films. In fact, higher doping levels lead to significantly lower carrier mobilities. This trend is in agreement with established models arguing that $Zn^{2+}$ and $Sn^{4+}$ can both act as ionized centers and scatter carriers strongly. Note also that at high Sn concentrations, where increases in Sn content have either negligible or negative effects on carrier concentration, mobilities are also depressed, sometimes dramatically. If IIS and LVS were the exclusive scattering mechanisms that influence carrier mobility, then mobility should not decline greatly after carrier concentration peaks since the density of ionized defects remains stable. The fact that carrier mobility continues to decrease with increased Sn content argues that another scattering mechanism may have a significant influence on carrier mobility. When further Sn doping no longer increases carrier concentration, the additional Sn atoms should no longer act as ionized centers, but instead act as neutral species. In the present case, the increasing quantity of Sn added to the $In_2O_3$ matrix forms increasing quantities of neutral species. This strongly argues that at high Sn doping levels, in addition to IIS and LVS, NIS is also an important factor in determining carrier mobility.

The increase in optical band gap with increasing carrier concentration in ZITO films can be readily attributed to a band filling-dependent Burstein−Moss shift.[21,58] The superior transparency of ZITO films in the near-IR range compared to that of ITO can then be ascribed to the relatively low carrier concentrations of the ZITO films.

**Polymer Light-Emitting Diode Response with ZITO Anodes.** $ZnIn_{2.0}Sn_{1.5}O_z$-based and ITO-based PLED devices having conventional PLED structures (Figure 10) were fabricated under identical conditions and in parallel. Surface cleaning and oxygen plasma treatment of both ZITO and ITO ensure that surface contamination is minimal. Thus, any differences in PLED response can only be explained by intrinsic differences in the anode materials. The conductivity of the commercial ITO films used in control devices was measured to be 4400 S/cm, about twice that of the $ZnIn_2Sn_{1.5}O_z$ film. The sheet resistance of ITO was 18 Ω/□, corresponding to a thickness of 130 nm. The sheet resistance and thickness of $ZnIn_2Sn_{1.5}O_z$ films were 24 Ω/□ and 200 nm, respectively. Considering the small emissive area (~10 $mm^2$) of the devices, such sheet resistance should not lead to a large voltage drop across TCO surface. Thus, there is no reason to believe that the thickness of anode

(51) Kostlin, H.; Jost, R.; Lems, W. *Phys. Status Solidi A* **1975**, *29*, 87.
(52) Frank, G.; Kostlin, H. *Appl. Phys. A* **1982**, *27*, 197.
(53) Chen, M.; Pei, Z. L.; Wang, X.; Yu, Y. H.; Liu, X. H.; Sun, C.; Wen, L. S. *J. Phys. D: Appl. Phys.* **2000**, *33*, 2538.
(54) Hwang, J. H.; Edwards, D. D.; Kammler, D. R.; Mason, T. O. *Solid State Ionics* **2000**, *129*, 135.
(55) (a) Kim, H.; Pique, A.; Horwitz, J. S.; Mattoussi, H.; Murata, H.; Kafafi, Z. H.; Chrisey, D. B. *Appl. Phys. Lett.* **1999**, *74*, 3444. (b) Tahar, R. B. H.; Ban, T.; Ohya, Y.; Takahashi, Y. *J. Appl. Phys.* **1998**, *83*, 2631.
(56) Zhang, D. H.; Ma, H. L. *Appl. Phys. A* **1996**, *62*, 487.
(57) Tahar, R. B. H.; Tahar, N. B. H. *J. Appl. Phys.* **2002**, *92*, 4498.
(58) Burstein, E. *Phys. Rev.* **1954**, *93*, 632.

material would in any major way impact device response. Therefore, despite the fact that ITO is approximately twice as conductive as $ZnIn_{2.0}Sn_{1.5}O_z$, the difference in conductivity alone is not expected to significantly affect device response such as turn-on voltage and current−voltage characteristics.

Although the ZITO-based and ITO-based devices have similar current−voltage characteristics, the ZITO-based device has substantially higher light output, and hence higher current efficiency, than the ITO-based control device (Figure 11). The difference can be attributed principally to the chemical resistance of ZITO toward PEDOT-PSS and, to a lesser degree, ZITO vs ITO work function effects (see below). The etching of ITO by PEDOT-PSS and the subsequent In diffusion into organic layers has been identified as one of the factors contributing to device degradation and reduced performance in both PLEDs and small molecule OLEDs.[59] The fact that MOCVD-derived ZITO thin films are ∼10× less reactive with respect to PEDOT-PSS corrosion than commercial ITO films makes the $ZnIn_{2.0}Sn_{1.5}O_z$/PEDOT-PSS interface far more stable than the ITO/PEDOT-PSS interface. The increased interfacial stability suppresses the diffusion of In, which can serve as an exciton quenching center in the polymer emissive layer,[60] and should subsequently enhance device response. Also since PFO-based PLED devices are hole-injection limited,[34] better interfacial anode-organic contact over the electrode surface area should enhance efficiency-dependent hole injection.

Considering the reported high work function of $ZnIn_{2.0}Sn_{1.5}O_z$ films (5.2−5.4 eV versus ∼4.5 eV for ITO)[61] and its corresponding better energy alignment with PFO (HOMO: 5.9 eV), the hole-transporting PEDOT-PSS layer might at first seem redundant. However, given the highly hydrophilic surface of the $ZnIn_{2.0}Sn_{1.5}O_z$ films, with an advancing aqueous contact angle of 23° (similar to that of ITO), the PEDOT-PSS may also function in the device as an adhesion layer to increase contact between the anode and the highly hydrophobic PFO. Furthermore, it has been argued that, because of the near-metallic electronic structure of PEDOT-PSS, the work function of PEDOT-PSS (∼5.0 eV) should be essentially insensitive to the degenerately doped oxide substrate work function.[62] If this assessment is valid, then in devices that use PEDOT-PSS as the hole injection layer, the anode material work function should have minimal effects on device response arising from intrinsic injection barriers. This may explain why the expected effects of improved hole injection by using a high work function anode material, such as lowering of the turn-on voltage for the $ZnIn_{2.0}Sn_{1.5}O_z$-based device and attendant increase in current, are not immediately evident in this particular case. Further investigations are underway to utilize the high work function of $ZnIn_{2.0}Sn_{1.5}O_z$ in PLED devices, such as replacing PEDOT-PSS with a siloxane-based self-assembled monolayer or interlayer.

## Conclusions

Highly effective $Zn(hfa)_2$·diamine MOCVD precursors can be straightforwardly synthesized in a single-step aqueous-phase reaction. X-ray single crystal diffraction indicates that the diamine and two diketonate ligands form six-coordinate quasi-octahedral geometries about $Zn^{2+}$. The packing motif of the least volatile and highest melting complex, $Zn(hfa)_2$(*N*,*N*-DEA) (**4**), indicates extensive intermolecular hydrogen bonding in the crystal. All four complexes are more volatile than the conventional Zn precursor, $Zn(dpm)_2$. The viability of the lowest melting complex **3**, $Zn(hfa)_2$(*N*,*N*′-DEA), as an MOCVD precursor has been demonstrated in the efficient growth of Zn−In−Sn−O thin films. The conductivity of as-grown ZITO films is as high as 2150 S/cm, and the optical transmittance of the films is greater than 80% over a wide spectral range. After annealing in a vacuum, the conductivity reaches 2900 S/cm. It is proposed that neutral impurity scattering is important for films with high Sn content, judging from Hall effect measurements. Films with the nominal composition of $ZnIn_2Sn_{1.5}O_z$ can be used as anodes in PLED devices and achieve greater light output and higher current efficiency than comparable ITO-based devices, principally due in this case to ZITO's reduced reactivity toward PEDOT-PSS. Overall, ZITO is a promising candidate as an alternative TCO material to ITO in a variety of optoelectronic devices.

**Acknowledgment.** We thank the U.S. Display Consortium (USDC) and NSF (CHE-0201767) for support of this research. We thank the Northwestern Materials Research Center (NSF MRSEC DMR-0076097) for providing characterization facilities. We thank Dr. N. Wu of the Keck Interdisciplinary Surface Science Center at Northwestern University for assistance with the XPS measurements and Profs. T. Mason and K. Poeppelmeier for helpful discussions.

**Supporting Information Available:** Detailed crystallographic information for selected precursor complexes and detailed electrical and optical data of ZITO films (PDF, CIF). This material is available free of charge via the Internet at http://pubs.acs.org.

JA044643G

(59) (a) Lee, S. T.; Gao, Z. Q.; Hung, L. S. *Appl. Phys. Lett.* **1999**, *75*, 1404. (b) Kim, J. S.; Friend, R. H.; Cacialli, F. *Appl. Phys. Lett.* **1999**, *74*, 3084. (c) Schlatmann, A. R.; Floet, D. W.; Hilberer, A.; Garten, F.; Smulders, P. J. M.; Klapwijk, T. M.; Hadziioannou, G. *Appl. Phys. Lett.* **1996**, *69*, 1764.
(60) (a) Herold, M.; Gmeiner, J.; Schwoerer, M. *Acta Polym.* **1996**, *47*, 436. (b) Werner, E.; Meier, M.; Gmeiner, J.; Herold, M.; Brutting, W.; Schwoerer, M. *Opt. Mater.* **1998**, *9*, 109.
(61) (a) Cui, J.; Wang, A.; Edleman, N. L.; Ni, J.; Lee, P.; Armstrong, N. R.; Marks, T. J. *Adv. Mater.* **2001**, *13*, 1476. (b) Ni, J.; Graham, A.; Armstrong, N. R.; Marks, T. J. Unpublished results.
(62) (a) Kugler, T.; Salaneck, W. R.; Rost, H.; Holmes, A. B. *Chem. Phys. Lett.* **1999**, *310*, 391. (b) Greczynski, G.; Kulger, T.; Keil, M.; Osikowicz, W.; Fahlman, M.; Salaneck, W. R. *J. Electron Spectrosc. Relat. Phenom.* **2001**, *121*, 1. (c) Greczynski, G.; Kulger, T.; Salaneck, W. R. *J. Appl. Phys.* **2000**, *88*, 7187.